Title
Active spectroscopic measurements of the bulk deuterium properties in the DIII-D tokamak (invited).

Journal
The Review of scientific instruments, 83(10)

ISSN
0034-6748

Authors
Grierson, BA
Burrell, KH
Chrystal, C
et al.

Publication Date
2012-10-01

DOI
10.1063/1.4739239

Active spectroscopic measurements of the bulk deuterium properties in the DIII-D tokamak (invited)[a)]

B. A. Grierson,[1,b)] K. H. Burrell,[2] C. Chrystal,[3] R. J. Groebner,[2] D. H. Kaplan,[2] W. W. Heidbrink,[4] J. M. Muñoz Burgos,[5] N. A. Pablant,[1] W. M. Solomon,[1] and M. A. Van Zeeland[2]

[1]*Princeton Plasma Physics Laboratory, Princeton, New Jersey 08543, USA*
[2]*General Atomics, P.O. Box 85608, San Diego, California 92186-5608, USA*
[3]*University of California San Diego, La Jolla, California 92093, USA*
[4]*University of California Irvine, Irvine, California 92697, USA*
[5]*Oak Ridge Institute for Science Education, Oak Ridge, Tennessee 37831-0117, USA*

(Presented 7 May 2012; received 4 May 2012; accepted 9 July 2012; published online 1 August 2012)

The neutral-beam induced D_α emission spectrum contains a wealth of information such as deuterium ion temperature, toroidal rotation, density, beam emission intensity, beam neutral density, and local magnetic field strength magnitude $|\mathbf{B}|$ from the Stark-split beam emission spectrum, and fast-ion D_α emission (FIDA) proportional to the beam-injected fast ion density. A comprehensive spectral fitting routine which accounts for all photoemission processes is employed for the spectral analysis. Interpretation of the measurements to determine physically relevant plasma parameters is assisted by the use of an optimized viewing geometry and forward modeling of the emission spectra using a Monte-Carlo 3D simulation code. © *2012 American Institute of Physics*. [http://dx.doi.org/10.1063/1.4739239]

I. INTRODUCTION

One popular means of measuring the ion temperature, density, and toroidal rotational velocity in deuterium neutral beam heated tokamak discharges with deuterium fueling is active charge-exchange recombination (CER) spectroscopy. This technique exploits the charge-exchange reaction between a high energy neutral donor atom from neutral beam injection (NBI) and a thermal impurity ion species in the plasma.[1–3] Spectroscopic measurements represent an "apparent" temperature and line-of-sight velocity that is different from the true temperature and velocity of the emitting ion. The apparent values from the impurity species must be corrected for energy-dependent atomic cross-section distortions[4,5] in order to infer the true impurity temperature, velocity, and density. Impurities are chosen for measurement due to the relative simplicity of the emission spectrum, and the thermal deuterium properties are inferred from the impurity measurements.

Previous direct measurements of the bulk deuterium properties from D_α spectra[6–8] exposed a number of issues relating to the technique. Some of these issues are as follows: (i) bright emission originating from plasma edge neutrals, (ii) halo emission from multiple charge-exchange reactions,[9] (iii) cross-section distortions due to the energy dependence of the charge-exchange cross section, (iv) finite lifetime of excited states, and (v) overlapping features in the spectral range, all contributing to uncertainties in the interpretation of the spectral fits. Underpinning this uncertainty is a failure to quantify the beam emission intensity and thermal charge-exchange intensity required for accurate interpretation of the measurement. Uncertainty (i) is significantly reduced with a large plasma-wall gap and no neutral fueling during the measurement, and operation in ELM-free H-mode. Uncertainty (ii) is reduced by full 3D simulation of the halo spatial diffusion and emission, and comparisons with direct halo measurements. Uncertainties (iii), (iv) are reduced by time-dependent collisional radiative modeling of non-equilibrium excited neutral emission, and uncertainty (v) is reduced by timeslice subtraction of high-speed measurements and a comprehensive spectral fitting model incorporating all known emission features described in Ref. 10. Advances in CCD technology have also increased the signal to noise ratio and quality of the measured spectral emission. The technique is supplemented by detailed knowledge of the content of impurity ions and fast ions from NBI in the plasma and a mature suite of complimentary diagnostics for integrated modeling.

This article describes advances on the measurement and modeling of the active D_α emission spectrum for the purpose of direct measurement of the thermal deuterium properties of temperature, density and toroidal rotational velocity, detailing the basis for results presented in Refs. 10 and 11. Measurements are made using modulated NBI to discriminate the core localized "active" emission from the passive edge emission by timeslice subtraction. Simultaneous measurements from both co-current and counter-current NBI provide a strong constraint on the true rotational velocity. A full three-dimensional time-dependent collisional radiative model[12] is employed for complete and detailed forward modeling of all active photoemission processes.

[a)]Invited paper, published as part of the Proceedings of the 19th Topical Conference on High-Temperature Plasma Diagnostics, Monterey, California, May 2012.

[b)]Author to whom correspondence should be addressed. Electronic mail: bgriers@pppl.gov.

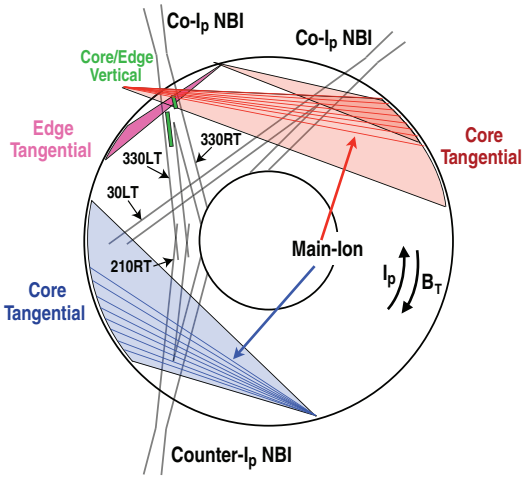

FIG. 1. Plan view of neutral beams and CER sightlines. [Adapted from and reprinted with permission from B.A. Grierson, *et al.*, Phys. Plasmas **19**, 056107 (2012). Copyright 2012 American Institute of Physics.]

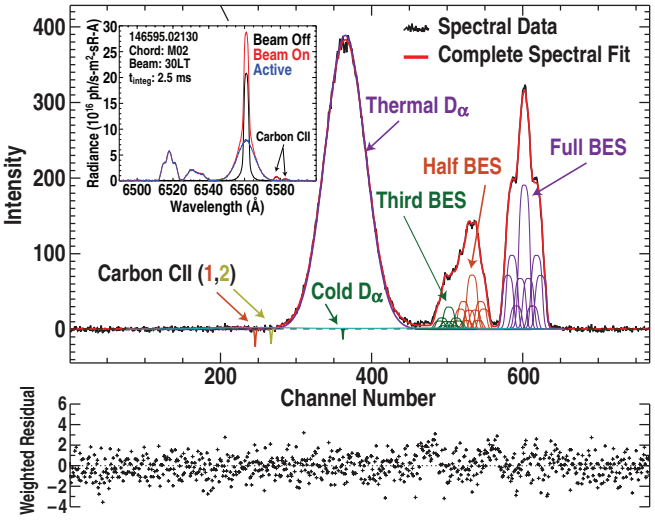

FIG. 2. Timeslice subtraction to obtain active emission (inset). Complete spectral fit for active spectrum incorporating all known emission features.

II. EXPERIMENTAL CONFIGURATION AND DIAGNOSTIC SPECIFICATIONS

Active charge-exchange recombination (CER) spectroscopy on DIII-D (Ref. 13) uses fiber optic viewchords of six of the eight neutral beamlines, displayed in Fig. 1. The main-ion CER diagnostic covers 1.70–2.19 m of the co- and counter-current NBI, with 8 sight lines on each beam (16 total viewchords). Main-ion CER and carbon CER viewchords exist at matched radii pairs.

Four McPherson model 207 2/3-m scannable spectrometers with custom asymmetric coma correction are used for spectral dispersion with 1200 g/mm ruled gratings. Each spectrometer accepts four fibers. Two Sarnoff SRI Avanti-768 CCD cameras are mounted "face-to-face" horizontally inside each spectrometer body with a 90° silver coated prism mirror between the cameras, reflecting the fiber images from the focusing mirror both up and down in pairs. The cameras have a 768 × 256 pixel configuration with 18 μm square pixels. At 6561.03 Å the reciprocal dispersion is 0.18 Å/pixel. The system is typically run with 2.5 ms integration, although high speed acquisition at 100 μs is possible.

Timeslice subtraction is used to extract the active emission localized to the region of the plasma where the viewchord and neutral beam cross. An example of spectra demonstrating the technique of timeslice subtraction is displayed in Fig. 2.

III. NEUTRAL BEAM

It is critical to accurately describe the NBI geometry, shape, power and injected current fractions in order to interpret photoemission intensities, and to guarantee consistency amongst neutral beam models. Current implementations of neutral beam models are used for three primary purposes: (i) computing profiles of carbon density from the impurity CER system using a "pencil" beam model, (ii) NUBEAM (Refs. 14 and 15) Monte-Carlo method called from TRANSP (Ref. 16) analysis for computing the injected neutral density, attenuation, beam-ion birth profiles, buildup of beam ion density, and pitch-energy resolved distribution function, and (iii) FIDAsim (Ref. 12) 3D Monte-Carlo simulations of beam neutral injection, attenuation, halo spatial diffusion, and the resulting photoemission from beam excited states, direct charge-exchange, halo emission and fast-ion charge exchange. Neutral beam descriptions (Gaussian height, width, and divergence) are obtained from in-vessel laser alignment and fast-camera imaging.[17]

A. Beam into gas

Injection of a neutral beam into a low pressure gas-filled tokamak reveals the characteristics of the neutral beam source without measurable attenuation or Stark-splitting of the emission lines. Beam-into-gas measurements without and with toroidal field have three primary functions for main-ion CER: (i) determination of the shape of the neutral beam emission spectrum for a "beam profile" used for Stark analysis,[18–20] (ii) evaluation of the accuracy of the spatial calibration through Doppler line shifts of all viewchords for a single beam neutral injector voltage,[21] and Stark splitting of the beam emission for beam into gas with toroidal field, and (iii) evaluation of the dynamic and steady-state mix of fractional current injected for the full, half and third energy components extracted from the beam ion source.[22] Photoemission from thermal deuterium charge exchange is more sensitive to the fractional density of full, half and third energy components because the cross-section peaks at lower relative velocity than carbon, which is sensitive to the full energy. An example of the dynamic change in beam neutral density over a heating beam "blip," typically used for diagnostic purposes, is displayed in Fig. 3 for NBI pulses into deuterium neutral gas at 81 kV. Evolution of the fractional neutral beam current for each energy components is highly reproducible, and analytic formulas for this evolution are used in modeling.

IV. DIRECT CHARGE-EXCHANGE AND HALO EMISSION

Thermal D_α emission is produced from two processes with fundamentally different origins. Direct charge exchange

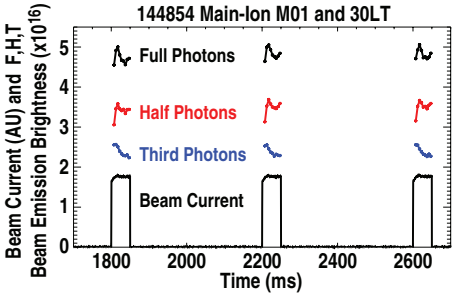

FIG. 3. High speed measurement of the beam emission from the three neutral beam energy components, full (black), half (red), and third (blue).

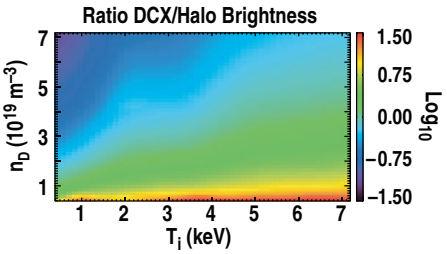

FIG. 4. FIDAsim lookup table of the ratio of DCX to halo emission brightness as a function of ion temperature and deuterium ion density.

[DCX, Eq. (1)] is the process of charge exchange from a beam neutral $D_b^0(n)$ in some principal atomic number n to a thermal ion $D_{th}(n')$ followed by photoemission. The direct charge exchange process is evaluated at the beam neutral velocity less the plasma rotational velocity with a proper Maxwellian averaged rate. Therefore, the DCX emission displays the cross-section distortions creating an "apparent velocity" which is different from the true rotational velocity,[4,5]

$$D_b^0(n) + D_{th}^+ \rightarrow D_b^+ + D_{th}^0(n') \quad \text{DCX}, \tag{1}$$

$$D_{th}^0(n) + D_{th}^+ \rightarrow D_{th}^+ + D_{th}^0(n') \quad \text{Halo}. \tag{2}$$

The product of the direct charge emission is a thermal neutral $D_{th}^0(n')$ which possesses a finite lifetime. This first thermal neutral, which travels ballistically, is now available for a second charge-exchange reaction with the thermal ions, if it is not ionized first. Mean-free path for a ballistic thermal neutral is determined by the probability of ionization by electrons, ions and impurities. When a second charge exchange reaction occurs, the first halo neutral is formed [Eq. (2)]. Because the charge capture can occur in any gyro-phase, the halo eventually occupies a larger physical volume than the beam through random-walk. The interaction relative velocity of the halo formation is thermal-thermal, hence the halo does not suffer from the cross-section distortions associated with the highly directed beam neutrals. Halo emission intensity is determined by the density of halo neutrals and the fractional occupation of the $n = 3$ level, which is largely determined by the thermal deuterium density, electron density and temperature. The ratio of direct charge-exchange emission intensity to halo emission intensity is displayed graphically in Fig. 4 for a mid-radius tangentially viewing main-ion CER viewchord.

It is clear from Fig. 4 that in low temperature discharges, increasing the plasma density increased the halo emission intensity, seen by the approximately 10% ratio of DCX/halo emission. In contrast, low density plasmas with appreciable ion temperatures are dominated by DCX emission. Figure 4 also indicates that the two processes are the same order of magnitude for a large range of plasma conditions.

The combination of direct charge-exchange and halo emission occurs as a single feature in the D_α emission spectrum. Modeling with FIDAsim shows that the Doppler shift from the cross-section distortion is not sufficiently shifted from the halo emission to be un-ambiguously fit as two separate Gaussians. Therefore, the interpretation of the measured Doppler shift "apparent velocity" depends strongly on the ratio of the emission intensity of one process compared to the other. In the DCX limit, there are strong cross-section distortions. In the halo limit, the apparent velocities are very near the true velocities, but the spatial resolution is compromised. It is this uncertainty which has confounded previous attempts to accurately determine main-ion parameters from active main-ion spectroscopy in deuterium plasmas. Uncertainty in the DCX/ Halo ratio is overcome in the present study by two methods: (i) direct measurement of the halo emission and (ii) views of both co- and counter-current NBI.

A. Direct measurement of halo emission

Halo emission exists in a spatial volume larger than the neutral beam. Core vertical viewchords displayed in Fig. 1 are oriented underneath one of the neutral beams, with another beam adjacent. When the perpendicular beam is fired into gas, no measurable beam emission is detected from the core vertical views. Thus any thermal D_α emission detected when this neutral beam is injected originates from the spatially larger halo. This viewing configuration permits a direct measurement of the neutral halo. An experiment was performed whereby the central vertical viewchords were tuned to D_α, and the neutral beam was modulated in time to enable timeslice subtraction.

Figure 5 displays the midplane values of halo, full energy beam, DCX, and FIDA emission intensities, as well as the locations of the vertically viewing CER chords. It can be seen by comparing Fig. 5(a) and Figs. 5(b) and 5(c) that the halo has expanded to a volume larger than either the beam, or the DCX, which enables the halo measurement. FIDA emission is nonzero over the vertical sightlines, however the intensity of the FIDA emission is lower than the halo emission by well over an order of magnitude.

Active D_α emission was fit for the discharge and one such time at the highest plasma density is displayed in Fig. 6(a). Parameters of interested are noted in figure. Also included is the halo emission predicted by FIDAsim. Although there is significant scatter in the measured photoemission intensity and profile shape of the halo emission intensity are reasonably well captured, however FIDAsim under-predicts the amount of halo emission. Halo emission intensity profiles are largely determined by the neutral beam attenuation, in keeping with

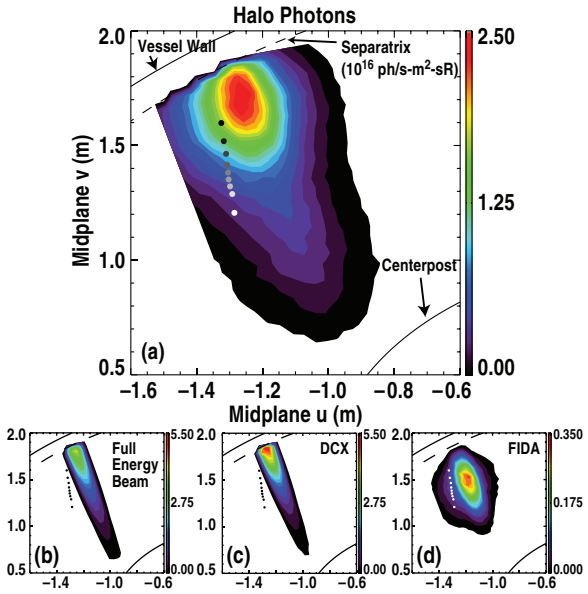

FIG. 5. Midplane quantities of of photoemission computed from FIDAsim in DIII-D discharge 145241 at 02400 ms. Displayed are (a) halo, (b) beam, (c) DCX, and (d) FIDA emission intensity.

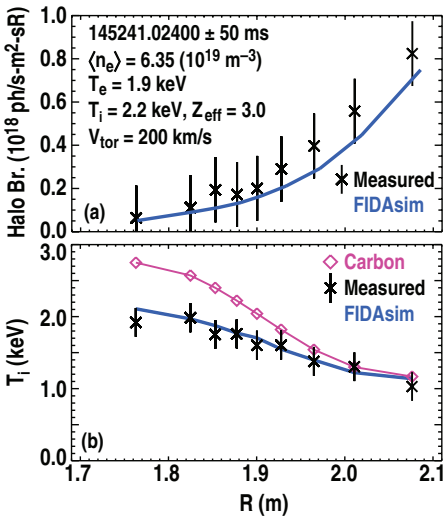

FIG. 6. Radial profiles of halo emission intensity and apparent temperature which is reduced due to spatial smearing.

simple considerations that the halo density is determined by the number of beam neutrals present to begin the multi-step halo creation and diffusion process, which is largely a function of the steep beam attenuation in plasma with a relatively flat density profile. An illustration of the spatial smearing effect on measured ion temperature incurred by vertically integrating through a volume which is much taller than it is wide is displayed in Fig. 6(b). The measured reduction in apparent ion temperature is consistent with the halo effect, not an actual reduction in the deuterium temperature. It is noteworthy that the tangential main-ion CER system does not suffer from such gross halo distortions, because the neutral beams are much narrower than they are tall. In principle, the measured halo emission contains the thermal deuterium poloidal velocity profile unaffected by the complexities of gyro-orbit cross-section corrections;[23] however, the spatial accuracy is compromised.

B. Combined cross section and halo effects

In order to accurately deduce the true velocity of an emitting ion species from the "apparent" velocity determined by the Doppler line shift obtained from a spectral fit, detailed knowledge of the viewing geometry, neutral beam characteristics and emission rate coefficient must be taken into account.[4,5] An alternate technique to determine the true rotational velocity is possible by having complimentary views of neutral beams which inject into the plasma in opposing directions.[24] Synthetic pure plasma profiles of electron and deuteron density and temperature were created and forward modeled in FIDAsim for creating a lookup table of corrections. One such profile is presented in Figs. 7(a)–7(c) for central density of $n_e = 2.5 \times 10^{19}(\mathrm{m}^{-3})$, zero toroidal rotation, and a relatively high central ion temperature of 8 keV to demonstrate conditions where the cross-section distortion will be significant. Figures 7(a)–7(c) present the input ion temperature profile and the temperature profile obtained from fitting the combination of halo and DCX photoemission spectra that have been added together; Fig. 7(b) contains the amount of photoemission from DCX and the halo which is predicted; Fig. 7(c) contains the input velocity (zero) and apparent toroidal rotational velocities from single-Gaussian

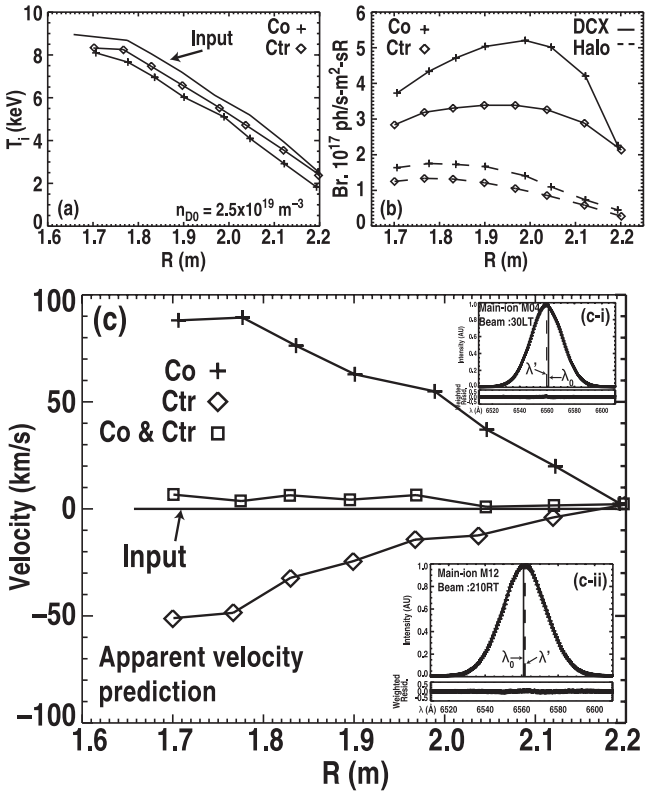

FIG. 7. FIDAsim predicted apparent velocities in a non-rotating plasma. (a) Input and synthetic diagnostic ion temperature profiles. (b) FIDAsim predicted DCX and halo brightness. (c) FIDAsim predicted apparent velocities for a non-rotating plasma, as well as co- and counter-view correction. (c)-(i) Displays synthetic spectrum for co-view and (c-ii) displays synthetic spectrum for counter-view.

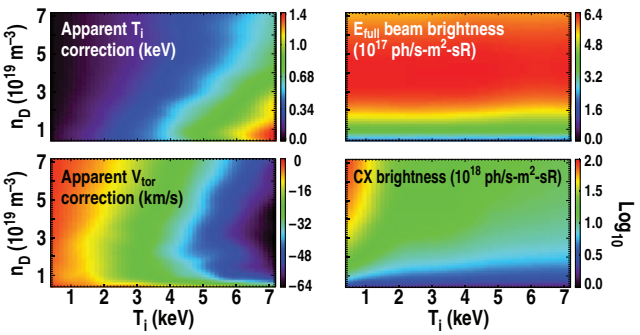

FIG. 8. FIDAsim lookup table using ideal plasma profiles for mid-radius main-ion CER sightline of beam 30LT. Displayed are correction values for temperature and velocity. Lookup is based on measured beam and total thermal charge-exchange brightness.

fits to the simulated spectra for co-current and counter-current views. Also contained in (c) is the result of applying the technique detailed in Ref. 23, identified as "Co & Ctr." Although the magnitude of the apparent velocities of the two views approaches 100 km/s, the co- and-counter correction technique provides the true velocity (zero) within typical quoted error estimates from main-ion CER of less than 10 km/s. There is also additional Monte-Carlo noise on the dominant DCX process contributing to the small amount of scatter. It is clear from Fig. 7(c) that the true velocity always lies between the apparent velocities measured by the two viewing systems.

In all cases, the view of the co-NBI has a larger distortion to the temperature and velocity than the ctr-view. This is attributed to the more perpendicular angle which the ctr-view possesses and consistent with the trends expected from cross-section distortions.[5] The simulated spectra for two central co- and counter-viewchords are given in Fig. 7(c-i) and 7 (c-ii) with overplotted fits and indicated Doppler shifts as dashed vertical bars. The fit residuals using a statistical weighting are included below the spectra and fits. For ion temperatures above 10 keV, distortions to the DCX spectra may become measurable above the signal-to-noise level. For this profile, the halo distortions (evaluated individually) display a weak (≈1 km/s) Doppler shift, which is negligible.

Databases of FIDAsim runs for ideal plasma profiles have been created for rapid assessment of expected cross-section corrections and for inferring the thermal deuteron density. A lookup table for a single sightline of co-NBI is presented in Fig. 8, which displays the temperature correction factor (T_i^{corr}) applied to apparent temperatures (T_i^{app}) from spectral fitting such that $T_i^{true} = T_i^{app} + T_i^{corr}$. The velocity correction is applied in a similar fashion, where for this view of a co-NBI is negative.

V. EXAMPLE DIAGNOSTIC PANEL

An example of the information provided by the main-ion CER spectroscopy system is displayed in Fig. 9 for an L-mode plasma. 4.4 MW of NBI provides a measurable fast

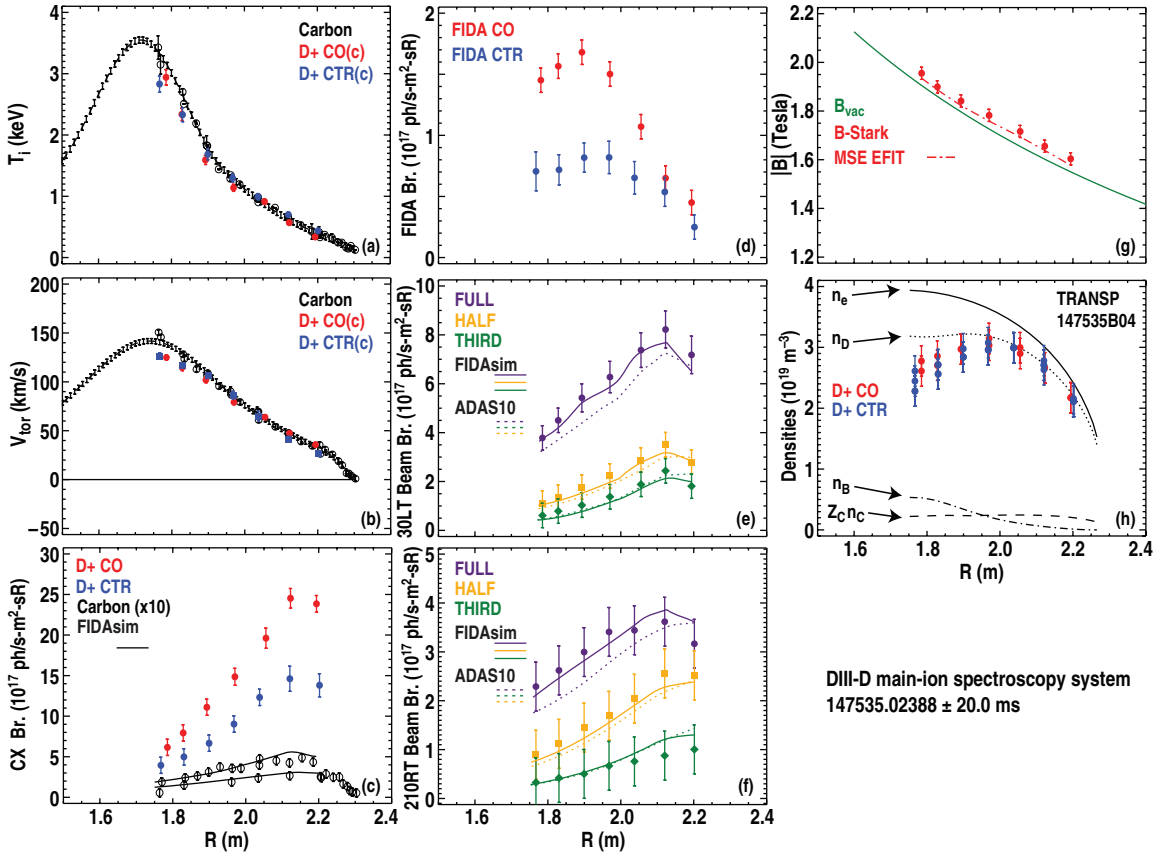

FIG. 9. Plasma parameters from carbon and main-ion CER profiles illustrating (a) ion temperature, (b) toroidal rotation, (c) thermal emission intensity, (d) FIDA emission intensity, (e) co-NBI, and (f) ctr-NBI beam emission intensity, (g) |**B**|, (h) plasma density constituents.

ion population. In Fig. 9(a) are carbon and deuterium ion temperature corrected for cross-section effects, as well as smooth spline fit to carbon data. Equal temperatures are seen across the profile except near the magnetic axis where perhaps some isotope effect is occurring. TRANSP analysis indicates approximately 100 eV lower deuterium temperature than carbon in these conditions with a large central beam-ion population. Figure 9(b) presents toroidal rotation with nearly equal velocities between carbon and deuterium, except for possibly near the magnetic axis where perhaps some measurable isotope effect is occurring. Figure 9(c) displays photoemission brightness for D^+ and CVI as well as forward modeling of carbon brightness with FIDAsim neutral beam deposition and excited states for two views. Figure 9(d) shows FIDA emission intensity, to be compared to orbit following calculations for beam-ion physics studies. Figure 9(e) and 9(f) display co-NBI and ctr-NBI measured brightness for each energy component, as well as FIDAsim and ADAS10 (Refs. 25 and 26) beam emission forward modeling demonstrating excellent agreement between modeled and measured emission. Figure 9(g) magnetic field strength from the B-Stark technique, magnitude of the vacuum toroidal field, and magnitude of total magnetic field from an MSE-based equilibrium reconstruction demonstrating good agreement. Figure 9(h) TRANSP+NUBEAM analysis profiles of electron density, thermal deuterium density, carbon density and deuterium beam ion density. Inferred thermal deuterium density from lookup table is also included and demonstrates core rollover due to high core beam ion density.

VI. CONCLUSIONS AND FUTURE WORK

This work details advances in the technique of charge-exchange recombination (CER) spectroscopy exploiting the large amount of information in the active D_α emission spectrum. Active spectroscopic measurements are fit with a complete model including thermal charge exchange, beam emission and fast-ion D_α (FIDA) emission self-consistently. Agreement displayed between measurements and modeling of the thermal emission, beam and re-neutralized fast ions, as well as cross-section corrections to apparent temperature and velocities represents a significant advancement in the usage of the active D_α spectrum as a plasma diagnostic tool. These advances in the technique have enabled accurate determination of thermal deuterium parameters of ion temperature, rotational velocity and density, as well as numerous other quantities related to beam deposition, equilibrium magnetic field strength, and the impurity concentration in the plasma. Extending the diagnostic capability to the steep gradient region of the H-mode pedestal is highly desirable but presents a challenge for measurement and modeling. However, with modern atomic calculations, integrated modeling tools and a mature suite of complimentary diagnostics the pedestal and edge region of the plasma has become a feasible next step.

ACKNOWLEDGMENTS

This work supported in part by the U.S. Department of Energy under DE-AC02-09CH11466, DE-FC02-04ER54698, DE-FG02-08ER54984, and SC-G903402. The author gratefully acknowledges useful discussions with R.E. Bell, M.J. Lanctot, R. Nazikian, and D.M. Thomas.

[1]R. Fonck, R. Goldston, R. Kaita, and D. Post, Appl. Phys. Lett. **42**, 239 (1983).
[2]R. Fonck, D. Darrow, and K. Jaehnig, Phys. Rev. A **29**, 3288 (1984).
[3]R. Isler, Plasma Phys. Control. Fusion **36**, 171 (1994).
[4]R. Howell, R. Fonck, R. Knize, and K. Jaehnig, Rev. Sci. Instrum. **59**, 1521 (1988).
[5]M. von Hellermann, P. Breger, J. Frieling, R. Konig, W. Mandl, A. Maas, and H. Summers, Plasma Phys. Control. Fusion **37**, 71 (1995).
[6]W. Mandl, *Technical Report JET-IR* (92)05, JET (1992).
[7]E. Busche, H. Euringer, and R. Jaspers, Plasma Phys. Control. Fusion **39**, 1327 (1997).
[8]T. Pütterich, E. Wolfrum, R. Dux, and C. Maggi, Phys. Rev. Lett **102**, 025001 (2009).
[9]J. Hogan, J. Nucl. Mater. **111**, 413 (1982).
[10]B. A. Grierson, K. H. Burrell, W. W. Heidbrink, M. J. Lanctot, and N. A. Pablant, Phys. Plasmas **19**, 056107 (2012).
[11]B. Grierson, K. H. Burrell, W. M. Solomon, and N. A. Pablant, Rev. Sci. Instrum. **81**, 10D735 (2010).
[12]W. W. Heidbrink, D. Liu, Y. Luo, E. Ruskov, and B. Geiger, Commun. Comput. Phys. **10**, 716 (2011).
[13]D. Thomas, G. McKee, K. Burrell, F. Levinton, E. Foley, and R. Fisher, Fusion Sci. Technol. **53**, 487 (2008).
[14]R. Goldston, D. McCune, H. Towner, S. Davis, R. J. Hawryluk, and G. Schmidt, J. Comput. Phys. **43**, 61 (1981).
[15]A. Pankin, D. McCune, R. Andre, G. Bateman, and A. Kritz, Comput. Phys. Commun. **159**, 157 (2004).
[16]R. J. Hawryluk, in *Physics of Plasmas Close to Thermonuclear Conditions*, edited by B. Coppi, G. G. Leotta, D. Pfirsch, R. Pozzoli, and E. Sindoni (CEC/Pergamon, Brussels, 1980), Vol. 1, p. 19.
[17]M. A. Van Zeeland, Plasma Phys. Control. Fusion **52**, 045006 (2010).
[18]N. A. Pablant, K. H. Burrell, R. J. Groebner, D. Kaplan, and C. T. Holcomb, Rev. Sci. Instrum. **79**, 10F517 (2008).
[19]N. Pablant, K. H. Burrell, R. J. Groebner, C. T. Holcomb, and D. H. Kaplan, Rev. Sci. Instrum. **81**, 10D729 (2010).
[20]N. Pablant, Ph. D. dissertation, University of California, San Diego, 2010.
[21]C. Giroud, A. G. Meigs, C. R. Negus, K.-D. Zastrow, T. M. Biewer, T. W. Versloot, and J.-E. Contributors, Rev. Sci. Instrum. **79**, 10F525 (2008).
[22]D. M. Thomas *et al.*, Rev. Sci. Instrum. **83**, 10D518 (2012).
[23]W. M. Solomon, K. H. Burrell, P. Gohil, R. J. Groebner, and L. Baylor, Rev. Sci. Instrum. **75**, 3481 (2004).
[24]W. M. Solomon, K. H. Burrell, R. Feder, A. Nagy, P. Gohil, and R. J. Groebner, Rev. Sci. Instrum. **79**, 10F531 (2008).
[25]See http://www.adas.ac.uk for ADAS atomic data and analysis structure. The originating developer of ADAS is the JET joint undertaking.
[26]M. O'Mullane, private communication (2012).